DTU Library

High temperature corrosion under conditions simulating biomass firing: depth-resolved phase identification

Okoro, Sunday Chukwudi; Montgomery, Melanie; Jappe Frandsen, Flemming; Pantleon, Karen

Published in:
Proceedings of EUROCORR 2014

Publication date:
2014

Document Version
Early version, also known as pre-print

Link back to DTU Orbit

Citation (APA):
Okoro, S. C., Montgomery, M., Jappe Frandsen, F., & Pantleon, K. (2014). High temperature corrosion under conditions simulating biomass firing: depth-resolved phase identification. In *Proceedings of EUROCORR 2014*

High temperature corrosion under conditions simulating biomass firing: depth-resolved phase identification

Sunday Chukwudi Okoro, Technical University of Denmark (DTU), Department of Mechanical Engineering, 2800 Kongens Lyngby, Denmark.
Melanie Montgomery, COWI A/S and DTU, Mechanical Engineering, Parallelvej 2, 2800 Kongens Lyngby, Denmark.
Flemming Jappe Frandsen, DTU, Department of Chemical and Biochemical Engineering, 2800 Kongens Lyngby, Denmark.
Karen Pantleon, DTU, Department of Mechanical Engineering, 2800 Kongens Lyngby, Denmark.

Summary

Both cross-sectional and plan view, 'top-down' characterization methods were employed, for a depth-resolved characterization of corrosion products resulting from high temperature corrosion under laboratory conditions simulating biomass firing. Samples of an austenitic stainless steel (TP 347H FG) were coated with KCl and isothermally exposed at 560 $^{\circ}$C for 168 h under a flue gas corresponding to straw firing. Scanning Electron Microscopy (SEM), Energy Dispersive Spectroscopy (EDS), and X-ray Diffraction (XRD) characterization techniques were employed for comprehensive characterization of the corrosion product. Results from this comprehensive characterization revealed more details on the morphology and composition of the corrosion product.

1   Introduction

The high corrosion rates of superheater tubes observed in boilers firing biomass are mainly caused by the condensation of alkali metal chlorides on these heat transfer surfaces. Such challenges have restricted the efficiency of biomass fired power plants, because they have to operate at low steam temperatures to avoid catastrophic failures [1]. As a result, there is a current need to properly understand the corrosion mechanisms, and subsequently, develop advanced materials dedicated to long-term applications in such challenging environments. Results from literature, both laboratory [2]–[5] and field studies [6], [7], have identified both Cl and K as corrosive species. The Cl has been proposed to degrade the alloy through an active-oxidation mechanism., As the corrosion process and environment during biomass firing is complex, it is difficult for field studies to give a detailed understanding of the corrosion mechanism. To gain precise information on a specific parameter, the corrosive environment in laboratory studies is often simplified in order to limit the complexity of corrosion products. In this work, realistic simulation of the corrosion of superheater tubes on a laboratory scale was carried out. The resulting complex corrosion product was thoroughly characterized using a novel approach of combining various characterization techniques to reveal the morphology and chemistry of the resulting corrosion product as a function of distance from the initial deposit surface.

2   Experimental

2.1   Sample preparation and exposure to biomass firing conditions

An austenitic steel tube of the steel TP 347H FG was investigated in this study. The alloy was determined by EDS to contain 18.1wt% Cr, 10.3wt% Ni, 2.0wt% Mn, 0.4wt% Si, 0.5wt% Nb and 68.7wt% Fe. The tube was cut into sections, degreased in acetone and ethanol before coating with a synthetic deposit slurry. The deposit slurry was made by mixing KCl with isopropanol. The coated specimens were exposed to conditions simulating straw firing in a corrosion test rig at 560 ^{o}C for 168 h. The rig consists of a gas mixing panel, an electrically heated horizontal furnace, and a gas cleaning system. 6% O_2, 12% CO_2, 400pmv HCl and 40ppmv SO_2 were fed from gas cylinders into the reactor using mass flow controllers. The gas composition was chosen to simulate the worst case flue gas composition in a straw fired power plant with respect to HCl. H_2O vapor was incorporated into the flue gas by passing the mixture of CO_2 and O_2 through a water bath before feeding it into the reactor. Nitrogen was used as a carrier gas. Fig 1 shows a schematic of the corrosion test rig.
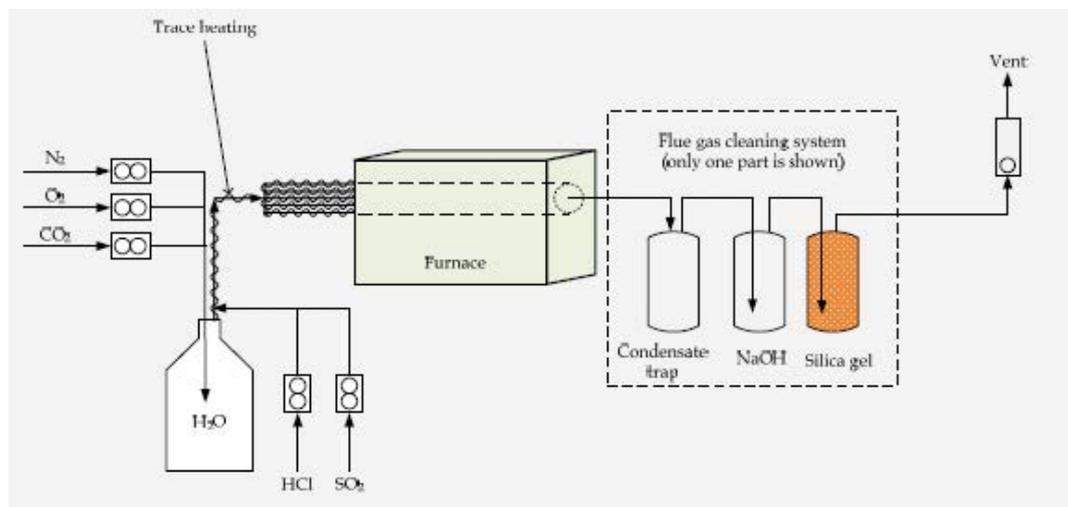

Figure 1: A schematic illustration of the corrosion test rig used for simulating high temperature corrosion during biomass firing.

2.2   Characterization of corrosion products

SEM, EDS, and XRD were employed for a comprehensive characterization of the resulting corrosion product. To obtain information on the morphology and chemistry of the corrosion product as a function of distance from the deposit surface, both cross section and plan view characterization methods were employed. Exposed samples were embedded in epoxy under vacuum and sectioned to expose the cross section. The cross sections were subsequently prepared metallographically down to 1µm diamond suspension, using water free solvents. SEM and EDS characterization were carried out on the prepared cross sections.

The plan view, 'top-down' characterization of the corrosion product started with investigation of the initial deposit of a non-embedded sample. This was followed by stepwise removal of the corrosion products using a scalpel or SiC paper, followed by subsequent characterization of the various surfaces revealed by successive layer

removal. Fig 2 shows a schematic of the plan view, 'top-down' characterization process. The blue arrows in the schematic show the directions from which investigations were carried out. The applied characterization techniques are also shown in relation to the investigated locations within the sample.
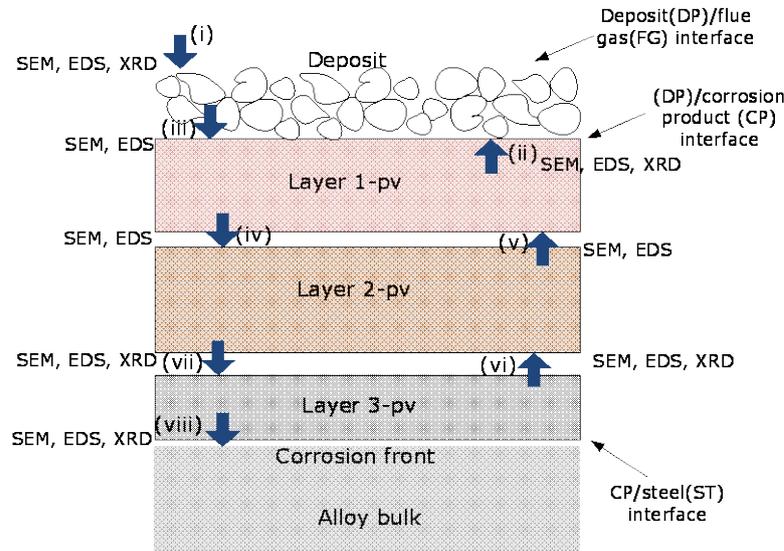

Figure 2: A schematic illustration of the plan view, 'top-down' characterization process employed for depth-resolved characterization of the corrosion product.

In both cross section and plan view characterization methods, SEM investigations were carried out using FEI (Inspect S) and JEOL (JSM 5900) microscopes operated at 15 kV. An Oxford Inca and Aztec EDS system attached to the SEM was employed for chemical element analysis. For XRD, a Bruker AXS diffractometer (Discover D8) was used with Cr-Kα radiation in grazing incidence geometry at an X-ray incidence angle of 3° (for measurements after layer removal) and 5° (for measurements on the original deposit surface).

3   Results and discussion

3.1   Cross section analysis of the exposed sample

A cross section of the corrosion product below the deposits is shown in Fig 3. Three layers of the corrosion product can be identified from the SEM image and the corresponding EDS maps show the composition of the different layers. The first layer (layer 1-cross section (cs)) consists of K, S, O and some Fe. The second layer (layer 2-cs) contains Fe, Cr and O. The third layer (layer 3-cs) consists of mainly Ni and S. The chemical element distributions, in the different layers suggest that the corrosion of the alloy proceeds according to the active oxidation mechanism, sustained by Cl [5], [8]. The sulphation of the deposit (KCl) by SO_2 (equation 1), is responsible for the formation of K_2SO_4 as observed in layer 1-cs. However such reaction also generates HCl/Cl (depending on the presence on H_2O).

$$2KCl + SO_2 + H_2O + 1/2O_2 \rightarrow K_2SO_4 + 2HCl \qquad (1)$$
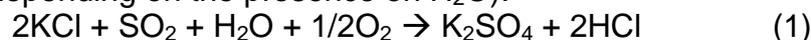
The Cl migrates to the bulk alloy and chlorinates the alloying elements. The metal chlorides formed are volatile, and consequently they evaporate towards the alloy deposit interface, where they are converted to metal oxides. The thermodynamics of the chlorination and the metal chloride-metal oxide transformation determines the mor-

phology and composition of the layers in the corrosion products. The elemental composition of the various layers forming the corrosion product agrees with thermodynamic predictions [9].
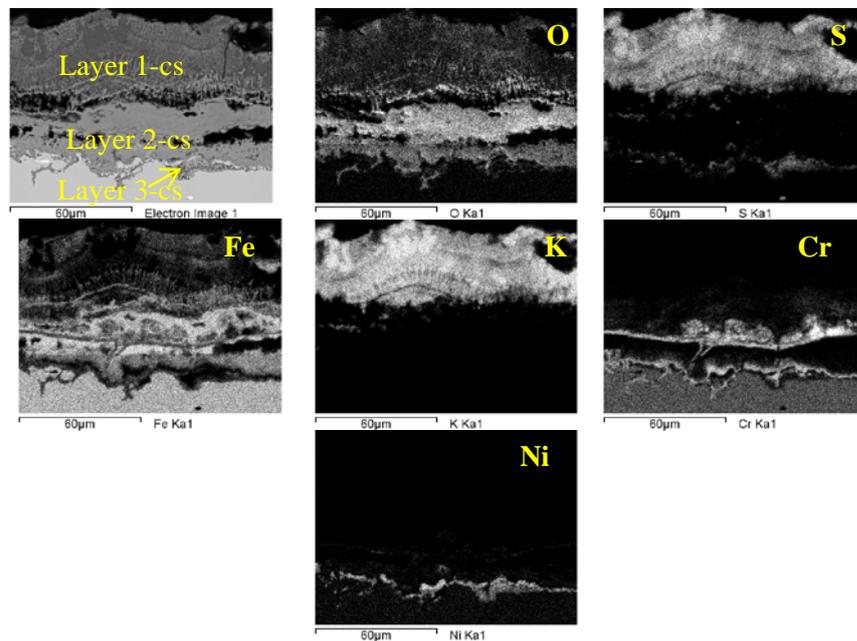

Figure 3: SEM image and corresponding EDS maps showing the distribution of the various elements across a cross section of the corrosion product.

3.2 Depth-resolved identification of corrosion product by plan view, 'top-down' approach

Plan view, 'top-down' characterization of the corrosion product allowed a comprehensive and complementary use of different techniques which resulted in an improved investigation of the morphology and chemical composition. In Fig 4, the morphology of the initial deposit is shown. It is seen that some particle clusters of changed chemical composition have accumulated around the initial KCl deposit. By EDS analysis, K, S and O have been identified on these particle clusters.
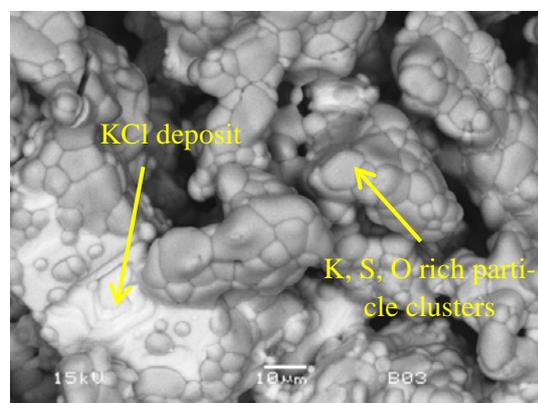

Figure 4: The initial deposit after exposure to simulated straw firing conditions.

The first layer of corrosion product (layer 1-plan view (pv)) as observed from plan view investigation is shown in Fig 5a. This is observed to consist of regions rich in K, Cl, Fe and O, and other regions rich in K, S, Fe and O
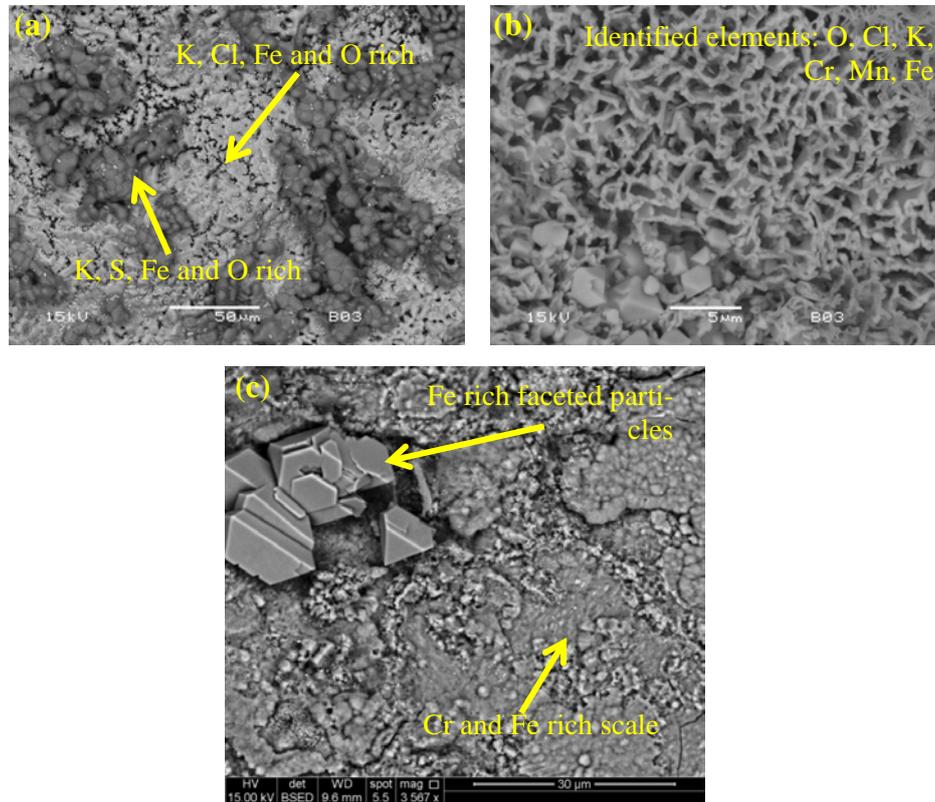

Figure 5: Corrosion product morphology as observed by plan-view 'top-down' investigations. (a): The first layer of corrosion product (layer 1-pv). (b and c): the second layer of corrosion product (layer 2-pv).

The elemental composition of the second layer (Figs. 5b and c) is similar to that observed from EDS maps in Fig 3. This layer consists predominantly of the oxides of the alloying elements of the investigated alloy. In Fig 6, the XRD results of qualitative phase analysis carried out at different locations on the corrosion product starting from the initial deposit surface are shown. The complementary use of results from EDS analysis supported identification of the crystalline phases present as a function of depth in the corrosion product. It is seen that both KCl and K_2SO_4 are present in the initial deposit after exposure to straw firing conditions. On the layer 2-pv of the corrosion product, Fe_2O_3 and $FeCr_2O_4$ are identified. This is in agreement with the elements identified by EDS analysis in Figs 5 (b-c).

Figs 7 (a-b) shows the selectively attacked regions presumably due to preferential attack of Cr and Fe where Ni is left behind as a skeleton. As the bulk of the alloy is approached through removal of the corrosion product by grinding, selective attack is observed to occur along grain boundaries. The elemental composition of layer 3-pv showed the presence of Cr, Fe, Ni and S. XRD diffraction measurements showed the presence of Ni_3S_2, which supports the identification of S and Ni bands in this layer as suggested from the EDS maps in Fig 3.
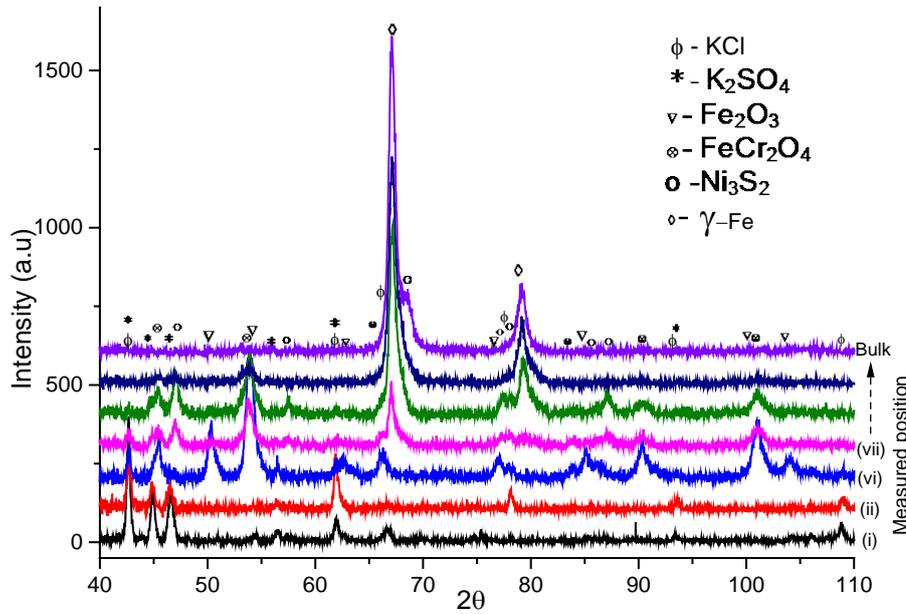
Figure 6: X-ray diffractograms recorded from different positions in the corrosion product after stepwise layer removal. The corresponding positions are shown in Fig 2.
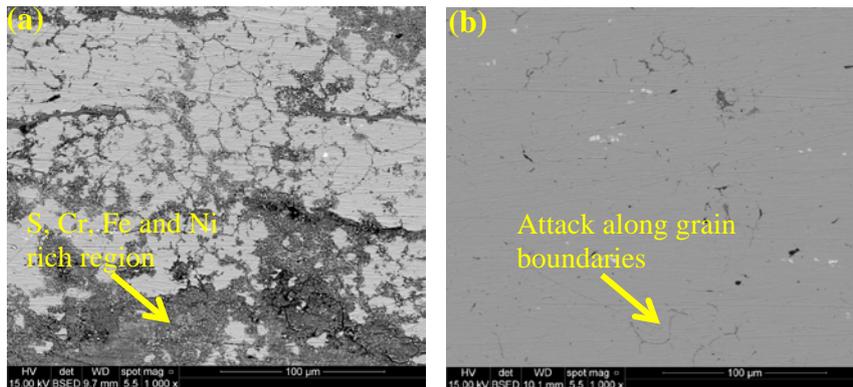

Figure 7: Selective attack on the third layer of corrosion product (a), and attack long grain boundaries at locations below layer 3-pv (b), as observed from plan view investigation.

The results from both cross-sectional and plan view, 'top-down' characterization of the initial deposit, corrosion product, and surface-near region of the alloy (corrosion front) showed preferential attack of Cr and Fe. In addition, the identification of Ni_3S_2 through plan view investigations suggests that sulphidation attack also occurred.

4   Conclusion

By complementary use of microscopic (SEM), spectroscopic (EDS) and diffraction (XRD), comprehensive characterization and identification of crystalline phases in the corrosion product formed on austenitic steel after exposure to straw firing conditions has been carried out. The use of a plan view, 'top-down' approach to characterize the corrosion product has given detailed insights on the depth-dependent morphology and chemical as well as phase composition of the corrosion product. This method

additionally allowed the identification of predominant crystalline phases by complementing EDS and XRD. The results highlight the release of Cl from the sulphation of the initial KCl deposit. This chlorine could then preferentially attack the iron and chromium at the corrosion front. Additionally some traces of sulphidation attack were observed.

Acknowledgements

5 References

[1] F. J. Frandsen, *Ash Formation , Deposition and Corrosion when Utilizing Straw for Heat and Power Production*. Doctoral Thesis, Kongens Lyngby: Department of Chemical and Biochemical Engineering, Technical Univeristy of Denmark, 2011, pp. 1–341.

[2] S. Sroda and S. Tuurna, "Laboratory scale tests on corrosion behavior of boiler materials in simulated combustion atmospheres (EU Project – OPTICORR)," *Mater. Corros.*, vol. 57, no. 3, pp. 244–251, Mar. 2006.

[3] J. Pettersson, N. Folkeson, L.-G. Johansson, and J.-E. Svensson, "The Effects of KCl, K_2SO_4 and K_2CO_3 on the High Temperature Corrosion of a 304-Type Austenitic Stainless Steel," *Oxid. Met.*, vol. 76, no. 1–2, pp. 93–109, 2011.

[4] S. C. Van Lith, F. J. Frandsen, M. Montgomery, T. Vilhelmsen, and S. A. Jensen, "Lab-scale Investigation of Deposit-induced Chlorine Corrosion of Superheater Materials under Simulated Biomass-firing Conditions," in *Eurrocorr*, 2008, vol. 23, no. 7, pp. 3457–3468.

[5] H. J. Grabke, E. and Reese, and M. Spiegel, "The effects of chlorides, hydrogen chloride, and sulfur dioxide in the oxidation of steels below deposits," *Corros. Sci.*, vol. 37, no. 7, pp. 1023–1043, 1995.

[6] M. Montgomery, S. A. Jensen, U. Borg, O. Biede, and T. Vilhelmsen, "Experiences with high temperature corrosion at straw-firing power plants in Denmark," *Mater. Corros.*, vol. 62, no. 7, pp. 593–605, 2011.

[7] L. A. Hansen, H. P. Nielsen, F. J. Frandsen, K. Dam-Johansen, S. Hørlyck, and A. Karlsson, "Influence of deposit formation on corrosion at a straw-fired boiler," *Fuel Process. Technol.*, vol. 64, no. 1–3, pp. 189–209, 2000.

[8] D. P. Miller, H. H. Krause, A. D. Vaughan, and K. W. Boyd, "The Mechanism in High Temperature Corrosion in Municipal Incinerators," *Corrosion*, vol. 28, no. 7, pp. 274–281, 1972.

[9] H. J. Zahs, A., Spiegel, M., Grabke, "The influence of alloying elements on the chlorine-induced high temperature corrosion of Fe-Cr alloys in oxidizing atmospheres," *Mater. Corros.*, no. 50, pp. 561–578, 1999.